Earthquake Research Advances 6 (2026) 100392

Contents lists available at ScienceDirect

Earthquake Research Advances

journal homepage: www.keaipublishing.com/en/journals/earthquake-research-advances

Assessing precursory signals with kinematic GNSS: Insights from the 2023 *M*w 7.8 Kahramanmaraş earthquake

Jingqi Wang [a,b], Rumeng Guo [a,*], Jianqiao Xu [a,b], Heping Sun [a,b]

[a] State Key Laboratory of Precision Geodesy, Innovation Academy for Precision Measurement Science and Technology, Chinese Academy of Sciences, Wuhan, 430077, China

[b] College of Earth and Planetary Sciences, University of Chinese Academy of Sciences, Beijing, 100049, China

ARTICLE INFO

Keywords:
High-rate GNSS
Kahramanmaraş earthquake
Accelerating exponential slip
Continuous data processing
Precursory signals

ABSTRACT

Identifying precursors of large earthquakes is critical for minimizing the losses of life and property. Recently, Bletery and Nocquet (2023) captured a ~2-h-long exponential acceleration of slip using the high-rate (5-min) Global Navigation Satellite System (GNSS) time series from the 48 hr before the 2011 M_W 9.0 Tohoku-oki earthquake, which was obtained by simply concatenating daily kinematic results together. Here, we apply their method to sum the horizontal displacements of 24 high-rate GNSS stations in the direction predicted by fault slip at the hypocenter of the 2023 M_W 7.8 Kahramanmaraş earthquake to characterize its precursory phase. Results demonstrate a several-hour accelerating exponential slip before the mainshock. However, considering that single-day processing would lead to discontinuities at the day boundary, we process the multi-day GNSS data in continuous mode, repeat the experiment, and find that the observed acceleration-like signals vanish. Our work shows that inadequate data processing may lead to the detection of false precursory signals, highlighting the need to develop robust processing techniques to identify reliable precursory signals before large earthquakes.

1. Introduction

Anticipating the approach of large earthquakes in advance could give populations enough time to "Drop, Cover, and Hold On" and greatly reduce losses of people lives and property safety (Bürgmann, 2023; Hirose et al., 2024; Lara et al., 2023). Both theoretical and laboratory studies suggested that large earthquakes commence with a stable, slow rupture that progressively accelerates into a dynamic and catastrophic rupture (Bletery and Nocquet, 2023; Bolton et al., 2023; Caballero et al., 2021; Kaneko et al., 2016; Shreedharan et al., 2020). Recently, there has been a renewed interest in studying slow aseismic slip preceding the mainshock, also known as preslip (Bouchon et al., 2011, 2013; Bowman and King, 2001; Dodge et al., 1996; Ruiz et al., 2014). However, tracking this short-duration precursor as a proxy of the impending large earthquake remains a challenge (Bedford et al., 2020; Bletery and Nocquet, 2025; Ellsworth and Bulut, 2018; Hirose et al., 2024; Pritchard et al., 2020; Roeloffs, 2006; Wang et al., 2024).

Recently, Bletery and Nocquet (2023) showed a systematic analysis of over 3 000 high-rate (5-min) Global Navigation Satellite System (GNSS) time series before 90 $M_W \geq 7.0$ global earthquakes, revealing a ~2-hr-long exponential acceleration of slip. If it can be proven that earthquake nucleation often involves an hours-long precursor phase, precursor warnings can be issued to save lives and injuries due to impending strong shakings. Note that Bletery and Nocquet (2023) presented the dot product stack for the 2011 M_W 9.0 Tohoku-Oki earthquake alone and observed an exponential-like signal at the scale of an individual earthquake. However, someone argued that this result may be attributed to network common mode error (CME) (Bletery and Nocquet, 2025; Bradley and Hubbard, 2023). Bletery and Nocquet (2025) proposed that while correcting the GNSS time series for CME could make the signal vanish, this common-mode filtering procedure may unintentionally remove an existing tectonic signal. To further examine the influence of CME and other potential factors, it is necessary to scrutinize the seismic records of other well-documented large events.

On February 6, 2023 at 1:17 UTC, the M_W 7.8 Kahramanmaraş (SE Türkiye) earthquake struck a seismic gap in the East Anatolian Fault Zone (EAFZ), followed approximately 9 hr later by a M_W 7.6 earthquake, which caused over 50 000 lives lost and 5 million people displaced in both Türkiye and Syria reported by the Disaster and Emergency Management Authority (AFAD) in Ankara, Türkiye (Jia et al., 2023;

* Corresponding author.
E-mail addresses: wjq_light@163.com (J. Wang), guorm@apm.ac.cn (R. Guo), xujq@asch.whigg.ac.cn (J. Xu), heping@whigg.ac.cn (H. Sun).
Peer review under the responsibility of Editorial Board of Earthquake Research Advances.

https://doi.org/10.1016/j.eqrea.2025.100392
Received 12 January 2025; Received in revised form 29 April 2025; Accepted 5 May 2025

Xu et al., 2023). This event, which exceeded expectations in terms of magnitude and damage, has drawn the attention of the community and seismologists around the world (Barbot et al., 2023; Mai et al., 2023; Melgar et al., 2023). Fortunately, there is a dense high-rate GNSS array in the epicentral area of the Kahramanmaraş event (Fig. 1), providing us with an excellent opportunity to characterize its precursory phase.

In this work, we apply the method of Bletery and Nocquet (2023) to detect the precursory signals of the 2023 Kahramanmaraş event. We then test the influences of different data processing strategies and CME on the results. Finally, we discuss other potential factors that may affect the precursory signals detected by high-rate GNSS.

2. Data and method

2.1. Data processing and model configuration

Receiver Independent Exchange (RINEX) data files near the hypocenter of the M_W 7.8 Kahramanmaraş earthquake are provided by the Türkiye Ulusal Sabit GNSS Ağı-Aktif (TUSAGA-Active) System. The PRIDE PPP-AR software (v3.0) (https://github.com/PrideLab/PRIDE-PPPAR) is invoked to process the GNSS data containing GPS and GLONASS two systems to obtain the 5-minute sampled kinematic time series, and undifferenced ambiguities have been resolved to obtain higher-precision results (Geng et al., 2019). We first use a single-day data processing strategy to obtain the kinematic time series. Notably, the 2023 Kahramanmaraş earthquake occurred near the UTC day boundary. Due to the discontinuities in satellite orbit, clock, and phase bias products across the day boundary, simply stitching together multiple single-day solutions can cause discontinuities in the coordinate time series (Geng et al., 2022). We thus employ a continuous processing strategy, where the data from the 48 hr prior to the earthquake are processed using the day-boundary discontinuity mitigated rapid products from Wuhan University (WUM0MGXRAP) within the same estimator (Geng et al., 2024), for more details refer to Table 1. Finally, given the potential impact of large data gaps on the accurate detection of precursory signals, we select 24 GNSS stations characterized by a data loss of less than 1% and the absence of significant steps or data gaps within the 2 hr preceding the earthquake. And we choose the mean value of the previous and subsequent observations to interpolate the missing data. We utilize GNSS data from stations located at 200 km, 300 km, 400 km, and 500 km from the hypocenter, applying stacking filtering to estimate CME for each distance range (Bian et al., 2021; Bradley and Hubbard, 2023). After deducting CME, the residual time series is used to calculate the stack time series. As shown in Fig. 2, different radius parameters have a little effect on the results. To minimize potential impacts as much as possible, 20 GNSS stations located beyond 200 km of the hypocenter are used to estimate the CME.

Given that the 2023 M_W 7.8 Kahramanmaraş earthquake initiated on an unmapped fault branch named the Nurdağı segment (NS) and then

Table 1
Models and estimation strategies for GNSS data processing.

Items	Descriptions
A priori noise	Pseudorange: 0.3 m; carrier phase: 0.003 m
Cut-off angle	10°
Observation weighting	$W = 1, \theta > 30°$; $W = 4\sin^2\theta, \theta < 30°$ where W is the scaling factor and θ is the elevation
Phase wind-up	Corrected
Tidal displacements	Solid Earth tide, ocean tidal loading, and pole tide
Ambiguities	Constants for each continuous observation arc
Zenith troposphere delays	Saastamoinen + Global Pressure/Temperature model; hourly constants with process noise of 1 cm/ $\sqrt{h}$ and Globel Mapping Function
Troposphere gradients	12-hourly constants with process noise of 0.005 m/ $\sqrt{12h}$ for the east and north components
Slant ionospheric delays	Random-walk parameters with process noise of 1 m/ $\sqrt{30s}$
Products	Day-boundary discontinuity mitigated rapid products from Wuhan University
Satellite orbit and clock	WUM rapid precise orbit (5 min interval) and WUM rapid precise clock (30 s interval)
Processing strategies	(1) Single-day processing; (2) Multi-day continuous processing

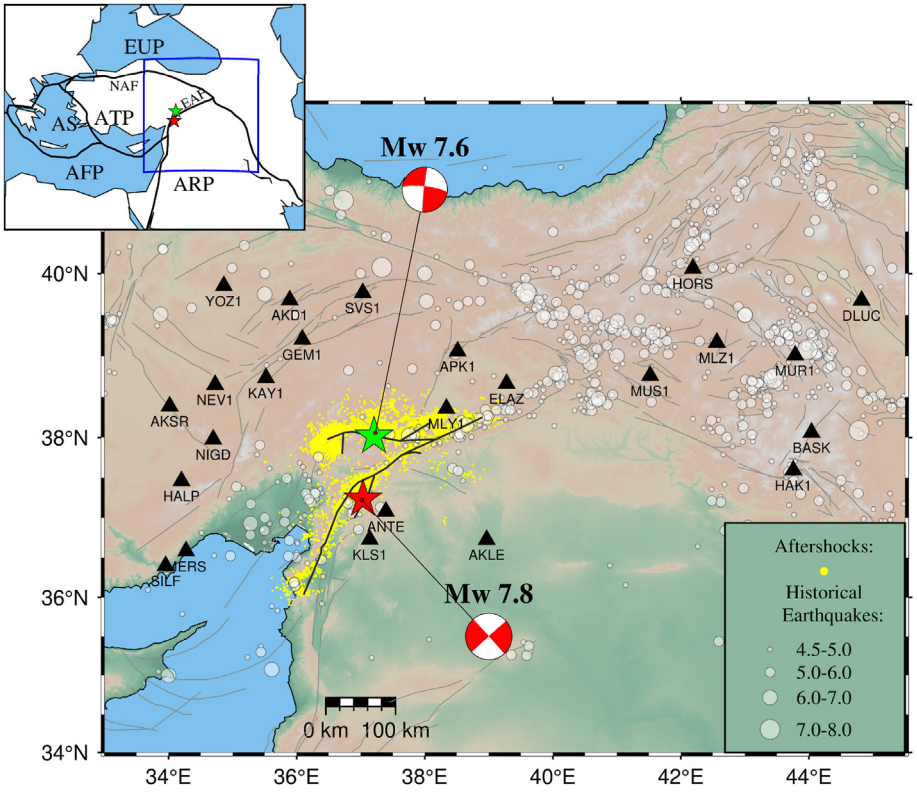

Fig. 1. Tectonic environment and distribution of high-rate GNSS stations surrounding the M_W 7.8 Kahramanmaraş earthquake. Red beachballs denote the focal mechanisms of the M_W 7.8 and M_W 7.6 earthquakes from the United States Geological Survey (USGS). The high-rate GNSS stations are marked by black triangles. The seismogenic faults are highlighted by black lines (Zhang et al., 2023), and other active faults are highlighted by gray lines (Emre et al., 2018). Yellow dots represent the relocated aftershocks within approximately a month following the M_W 7.8 and M_W 7.6 events. The transparent circles indicate historical earthquakes with $M > 4.5$ during the period 1900–2018 (Tan, 2021). The inset map delineates our study region within the large-scale tectonic framework. Abbreviations: AS (Aegean Sea), AFP (African Plate), ATP (Anatolian Plate), ARP (Arabian Plate), EUP (Eurasian Plate), NAF (North Anatolian Fault), and EAF (East Anatolian Fault).

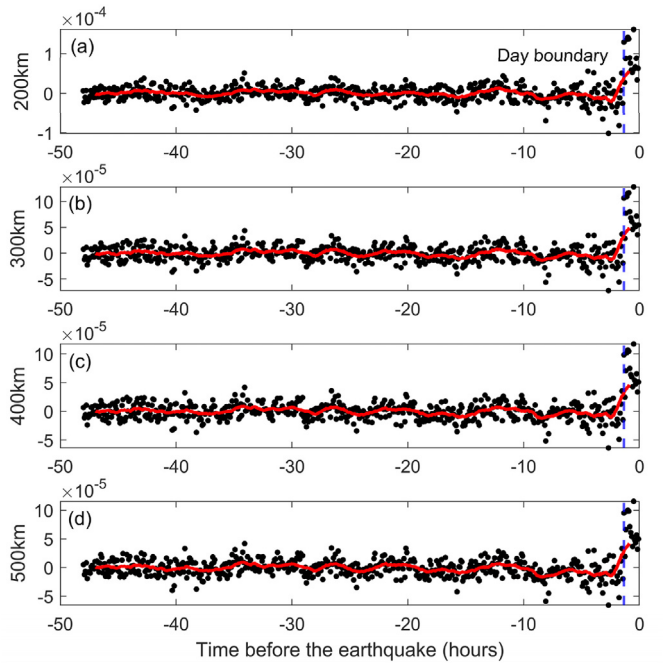

Fig. 2. The stack time series is calculated by cleaned time series which deducts CME with different distances. Panels (a)-(d) represent the stack time series calculated after removing CME calculated with the distances of 200, 300 km, 400 km, and 500 km from the hypocenter, respectively. The red line represents the moving average (time window: 1 h 50 min) on the [-48 h, -1 h 50 min] time period. The blue dashed lines indicate the day boundary.

propagated to the EAFZ, revealing a cascading rupture, it makes more sense to explore the precursory process using the equivalent focal mechanism (strike/dip/rake: 28°/85°/-1°) of the NS (https://earthquake.usgs.gov/earthquakes/eventpage/us6000jllz/finite-fault). The hypocenter location (37.238°N, 37.035°E) is from the relocated result of Anthony Lomax (Lomax, 2023).

2.2. Weighted stack and moment rate

We apply the method outlined in Bletery and Nocquet (2023) to define the value of 0 in the residual time series as the median of the 48 hr to 24 hr before the mainshock and subtract this median from the time series to obtain $\vec{u}_i(t)$. We consider a simple fault dislocation embedded in a homogeneous semi-infinite elastic half-space to calculate the expected displacements $\vec{g}_i$ at the GNSS stations. $\vec{g}_i$ is a vector indicating the expected displacement at station *i* if the fault starts to slip (by a unit of slip) at the hypocenter of the impending earthquake, in the direction of the upcoming slip. To limit the modeling errors caused by the nodal plane ambiguity, we choose an unrealistically small fault of 1 km by 1 km to be equivalent to the point source. For each GNSS station *i* at each time step *t*, we calculate the dot product of $\vec{u}_i(t)$ and $\vec{g}_i$ to test the existence of preslip. Displacements are generally larger near the source. If the preslip exists, the dot product will be positive. If $\vec{u}_i(t)$ and $\vec{g}_i$ are perpendicular, their dot product would be null, and there is no preslip. A natural weight emerges from computing the dot product with $\vec{g}_i$. If the station is close to the hypocenter, the norm of $\vec{g}_i$ and the amplitude of the dot product are larger than those of the stations far from the hypocenter. To test whether the GNSS stations near the hypocenter tend to move before the rupture as they did during the mainshock rupture, we estimate the expected horizontal displacements for each site induced by such earthquake precursors (Fig. 3).

The weighted stack time series $S(t)$ is computed with the stack of dot products divided by the noise amplitude. The noise amplitude on each GNSS station is estimated as the L2 norm of $\vec{u}_i(t)$ between 48 and 24 h before the earthquake $\sigma_i = \left\| \vec{u}_i(t_{[-48,-24]}) \right\|$ (Montagner et al., 2016; Rietsch, 1980).

$$S(t) = \sum_{i=1}^{N} \frac{\vec{u}_i(t) \cdot \vec{g}_i}{\sigma_i^2} \tag{1}$$

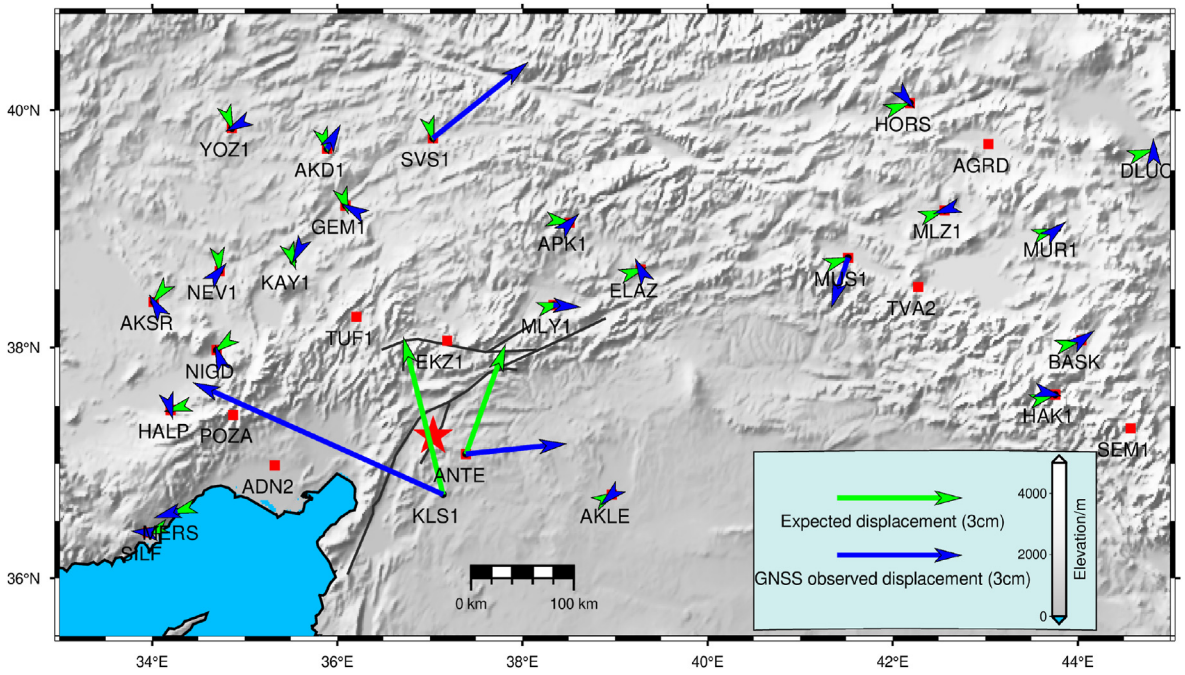

Fig. 3. The observed and expected displacements. The blue and green arrows represent median displacements in the 2 hr before the event with respect to the median position on the previous day observed by GNSS and the expected displacements, respectively. The red star represents the location of the hypocenter. The red squares represent the GNSS stations to estimate the possibility that the preslip signal is due to noise.

where N is the number of GNSS stations.

To compare with the released energy of the mainshock, we transform $S(t)$ to the cumulative moment of preslip using a coefficient of proportionality. Let $s(t)$ be the hypothetical precursory slip time series. The relationship between $s(t)$ and $\vec{u}_i(t)$ can be considered as,

$$\vec{g}_i s(t) = \vec{u}_i(t) \tag{2}$$

By dot product with $\vec{g}_i$ and dividing by σ_i^2 of Eq. (2), we can obtain the relationship between $s(t)$ and $S(t)$ with the stacking on all stations,

$$s(t)\sum_{i=1}^{N}\frac{\vec{g}_i\cdot\vec{g}_i}{\sigma_i^2} = \sum_{i=1}^{N}\frac{\vec{g}_i\cdot\vec{u}_i(t)}{\sigma_i^2} = S(t) \tag{3}$$

Defining $\sigma_g = \sum_{i=1}^{N}\frac{\vec{g}_i\cdot\vec{g}_i}{\sigma_i^2}$, Eq. (3) can be simplified to Eq. (4),

$$s(t) = \frac{S(t)}{\sigma_g} \tag{4}$$

Since we define the 1 km by 1 km fault to calculate $\vec{g}_i$, the value of $s(t)$ is not relevant. The relationship of the corresponding cumulative moment M_0 and $S(t)$,

$$M_0(t) = \mu LW s(t) = \frac{\mu LW}{\sigma_g}S(t) \tag{5}$$

where μ is the shear modulus, which is set as 29.353×10^9 Pa, L and W represent fault length and width, respectively, and $L = W = 10^3$ m.

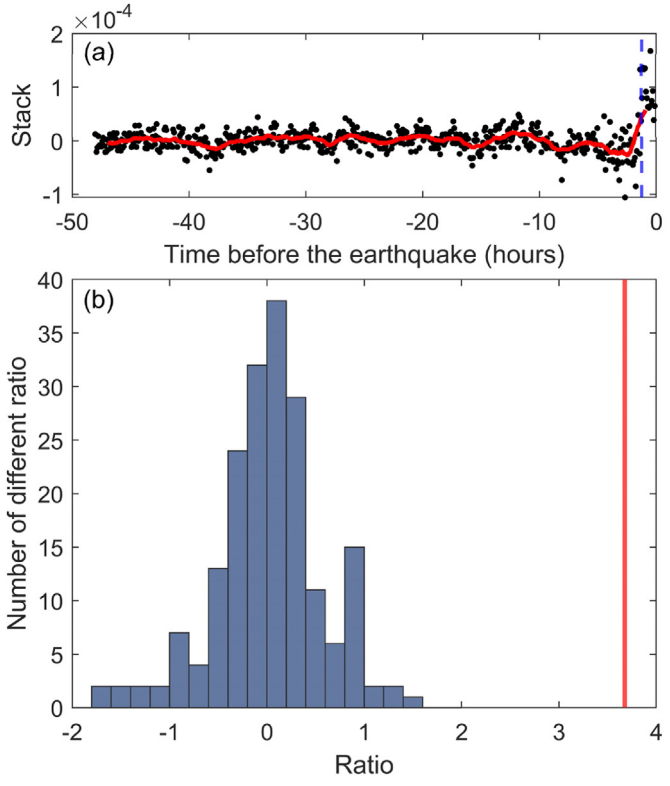

Fig. 4. The ratio between the last point of the moving average and the maximum in the two previous days. (a) Dot product stack of 24 GNSS time series. The red line represents the moving average (time window: 1 hr 50 min) on the [-48h, -1 h 50 min] time period. (b) The red line represents the ratio value of the 2023 Kahramanmaraş earthquake, and the bar chart shows the statistics of the ratio values calculated based on the hypothetical seismic event timing.

3. Results and discussion

3.1. Potential precursory signals before the 2023 Kahramanmaraş event

We first apply the method outlined in Bletery and Nocquet (2023) to stack the dot product between the kinematic time series (single-day data processing) and the expected displacements to verify the presence of preslip. Notably, $S(t)$, which is subtracted CME, could be modeled well by an exponential function $y(t) = a\exp\left(\frac{t}{\tau}\right) + b$ with a time constant τ of 0.8 h, revealing that the M_W 7.8 Kahramanmaraş earthquake exists an hours-long precursor as predicted by the laboratory experiments and numerical models. Such a short duration and exponential acceleration of slip make the precursory phase independent of slow slip events (Bletery and Nocquet, 2023). To compare with the released energy by the mainshock, we estimate the cumulative moment of the precursory slip by a coefficient of proportionality. The accumulated seismic moment before the rupture is $\sim 3.2 \times 10^{19}$ N·m, corresponding to an M_W 7.0 earthquake.

To reduce the effect of high-frequency noise on signal detection, we calculate a moving average (time window: 1 hr 50 min) of the dot product stack. It is found that the maximum of the moving average is the last point, and there is an obvious monotonically increasing a few hours before the mainshock (Fig. 4). The ratio of the last point to the maximum of the stack moving average in the last 2 days (excluding the latest 1 hr 50 min) is 3.67. To estimate the possibility that the preslip signal is due to noise, we utilize the aforementioned analysis on data from January 1, 2023, up to two days prior to the Kahramanmaraş earthquake. We collected 2 630 s GNSS data samples, excluding KLS1, with their locations illustrated in Fig. 3. However, there is the possibility of missing data and poor data quality at different stations on a daily basis. Considering the importance of the ANTE station in dot product stack, we deduct the blunders in the ANTE time series and allow other single-day data shortfalls of less than 2 h to participate in the dot product stack. The regularized expectation maximization (RegEM) method is used for data interpolation to ensure that the interpolated data maintains the same motion trend as the original data, thereby ensuring the robustness of the stack results (Li et al., 2019). The data from 48 hr before the origin time are used to calculate the dot product stack with the same strategy as in this study. We draw a random time within each 4-hr window, set it as the origin time for "fake earthquakes", and calculate the dot product stack in the 48 preceding hours. Then we compute the moving average and ratios

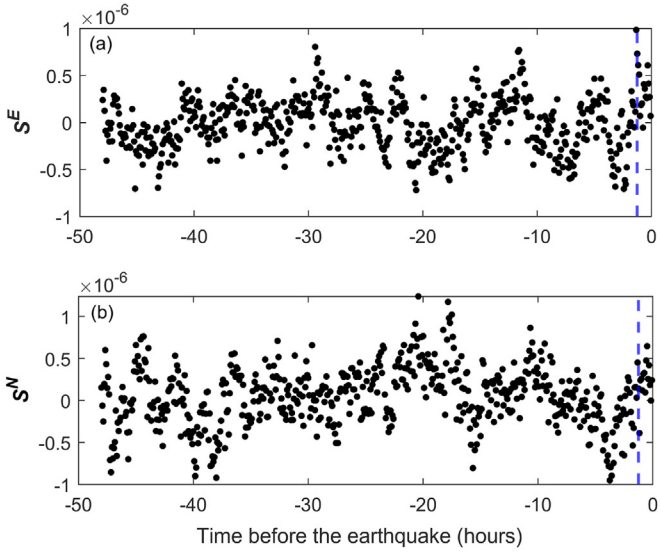

Fig. 5. Stack in the east and north directions. S^E and S^N represent the dot product stack of the GNSS time series preceding the M_W 7.8 Kahramanmaraş earthquake projected in the east and north directions, respectively.

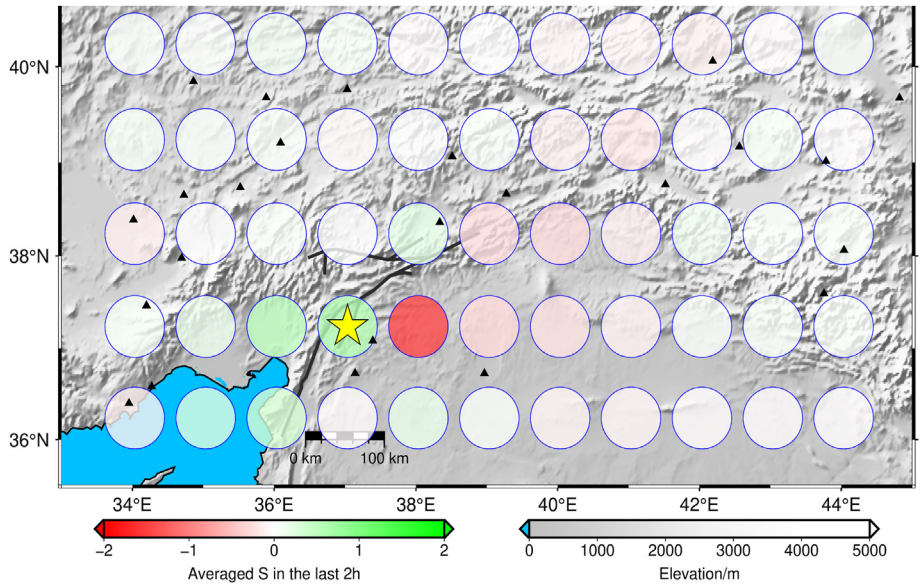

Fig. 6. Precursory signal detection at different source locations. The circles represent the normalized mean values over the last 2 hr of stacks, considering different source locations. The yellow star shows the epicenter of the M_W 7.8 earthquake. The black triangles are the GNSS stations.

of these "fake earthquakes". For the dot product stack of 192 "fake earthquakes", we calculate the ratio of its last point to the maximum of the previous 2 days with the same strategy. Notably, all ratios are much less than 3.67 (Fig. 4), indicating the specificity of the exponential acceleration of slip prior to the M_W 7.8 event.

To demonstrate that the precursory signal is associated with the fault slip of the impending Kahramanmaraş earthquake, we conduct a similar stacking analysis for the east and north directions. As depicted in Fig. 5, the stack time series reveals no precursory accelerating slip, indicating that the source signals $S(t)$ are attributed to processes taking place in the direct vicinity of the hypocenter. To further investigate the sensitivity of this signal to the source location, we calculate the average of the last 2 hr for the dot product stack considering different source locations and find that the largest value is obtained at the hypocenter of the Kahramanmaraş earthquake (Fig. 6).

3.2. Influence of common mode error

Since the publication of Bletery and Nocquet's results, informal discussions have emerged on various platforms. In particular, it has been suggested that correcting GNSS time series from network CME can cause both sinusoidal and exponential signals to disappear (Bradley and Hubbard, 2023). We thus test the effect of CME on our results. Fig. 7a and 7b demonstrate the stack time series with the single-day processing strategy without and with the subtraction of CME, respectively. It suggests that whether CME is subtracted or not, the stack time series $S(t)$ shows a smooth accelerating signal before the mainshock.

3.3. Influence of data processing strategies

Notably, although we have accounted for potential effects on signal detection and obtained surprising results, the results may not be robust. As shown in Figs. 8 and 9, it is found that the ANTE and KLS1 stations, which constitute a significant portion of the stack, exhibit discontinuities at the day boundary. The strategy of single-day processing to obtain GNSS time series from the 48 hr preceding the earthquake may impact the investigation of preseismic anomalies for this event. We thus change the data processing strategy to continuously process multi-day GNSS data with the PRIDE PPP-AR software using the WUM0MGXRAP. Fig. 9 shows that differences in data processing modes at the same station lead to significant discrepancies in the time series over the last 2 hr. Fig. 7c and d show the stack time series without and with the subtraction of CME, respectively, with the continuous processing strategy, revealing that there is no precursory accelerating slip, regardless of whether the CME

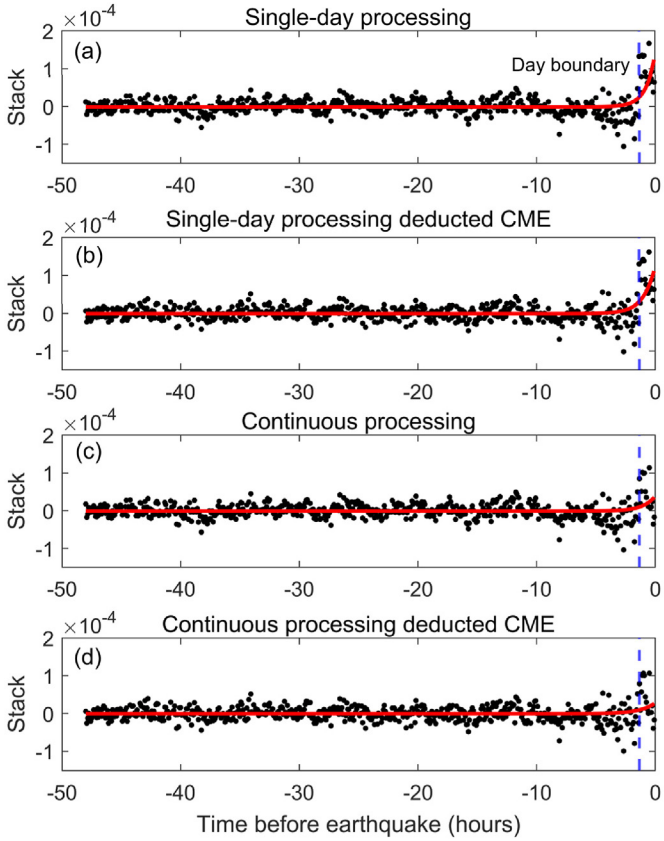

Fig. 7. Dot product stack of 24 GNSS time series and exponential fit with the nonlinear least-squares method (red line). (a) GNSS data obtained through the single-day processing strategy are incorporated into the stack calculation. (b) Subtract CME from (a). (c) GNSS data obtained through the continuous processing strategy are incorporated into the stack calculation. (d) Subtract CME from (c).

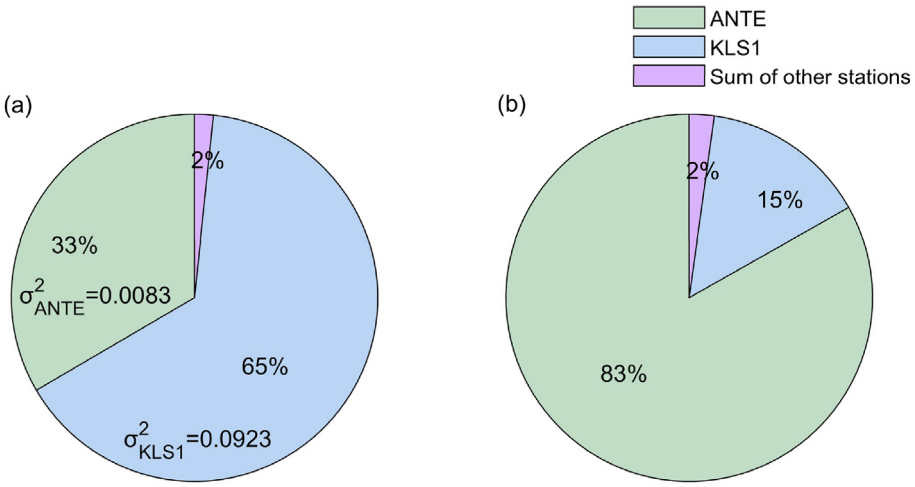

Fig. 8. The weight assigned to different GNSS stations and the time series with a significant proportion during stack calculations. The relative weight of the amplitudes of Green's functions (before (a) and after (b) divided by σ_i^2).

effects are removed. This highlights the importance of continuous data processing for detecting precursory signals of earthquakes occurring near the day boundary. And there is no significant preseismic slip that would lead to deformation exceeding the GNSS data noise level before the Kahramanmaraş event.

The seismic events occurring at the day boundary in the study of Bletery and Nocquet (2023) may be influenced by the data processing strategies employed. Some events occurring at the day boundary that are included in the global stack also exhibit steps at the boundary. For example, the 2018 M_W 7.4 earthquake that occurred on January 10 at 02:51 (UTC time), when included in the global stack with other events, may have a certain impact on the results. In addition, for the events excluded from their study, there are obvious steps at the day boundary in the stack time series. While this does not affect the results of the global stack, it can lead to significant misinterpretations when investigating the precursory anomalies of individual events. Similarly, the discontinuities in products such as clocks and orbits were not considered in the work of Bletery and Nocquet (2025).

3.4. Other potential factors

Although we have eliminated the influence of the CME and revised

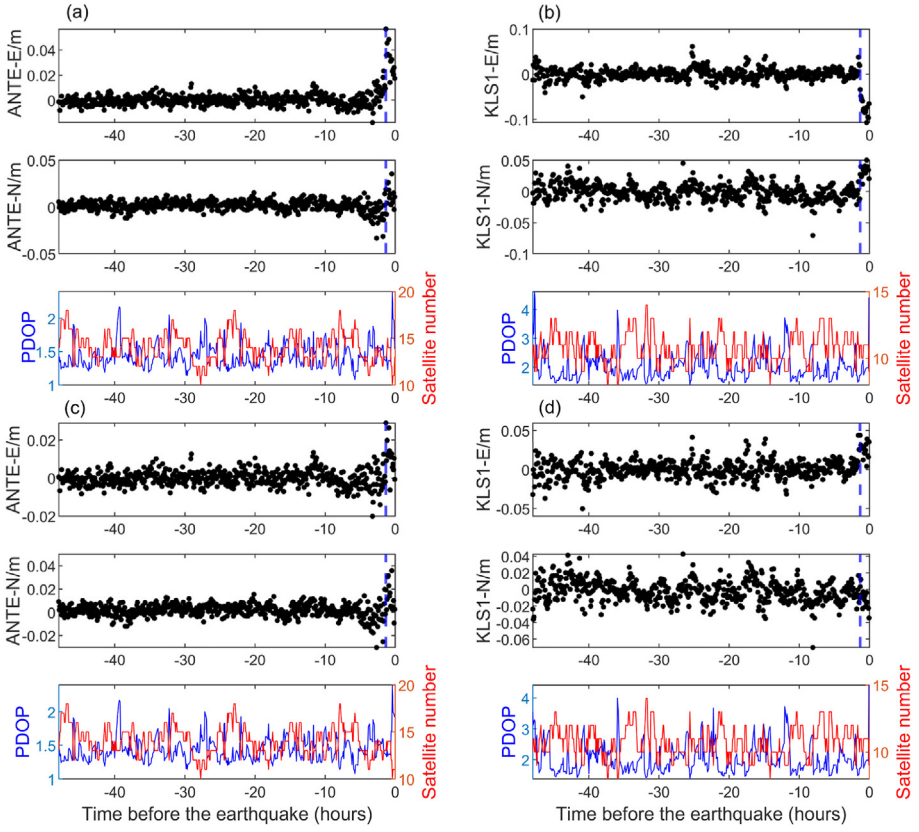

Fig. 9. The results obtained from the two GNSS stations with the largest proportions using different data processing strategies. (a) The horizontal time series of station ANTE is obtained through the single-day processing strategy, along with the satellite observations and PDOP values for each epoch. (b) The results for station KLS1 use the same strategy as (a). (c) The horizontal time series of station ANTE is obtained through the continuous processing strategy, along with the satellite observations and PDOP values for each epoch. (d) The results for station KLS1 use the same strategy as (c).

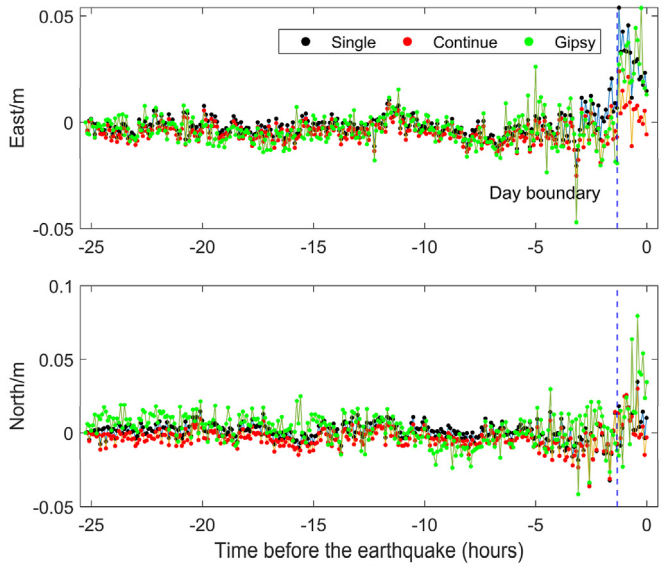

Fig. 10. Comparison of kinematic time series of ANTE calculated by PRIDE PPP-AR and Gipsy software. The black and red dots represent results calculated by the PRIDE PPP-AR software using single-day and continuous processing, respectively, while the green dots denote results computed using Gipsy.

the data processing strategy to confirm that no precursors are present before the 2023 Kahramanmaraş earthquake, there are still other factors may still influence the observed results. Data quality can significantly impact the results. Removing outliers from the time series or stations with poor data quality will help ensure the robustness of the findings such as the May 27, 2010 M_W 7.1 and March 25, 2012 M_W 7.1 events in the study of Bletery and Nocquet (2023). Additionally, in the stacked time series of certain individual seismic events, such as the July 15, 2009 M_W 7.7 and August 27, 2012 M_W 7.4 earthquakes, a precursory phase of accelerating slow slip is observed. However, such a phenomenon does not occur exclusively before the mainshock but is also accompanied by a clear daily periodicity in the time series. We argue that this periodicity may be attributed to multipath error. Notably, both far-field and near-field GNSS stations are crucial for detecting the precursory phase. Given the relatively small size of the earthquake nucleation zone, near-field GNSS stations are employed to capture precursory signals, while far-field stations are used to calculate the CME and correct the near-field data accordingly.

Furthermore, we have compared the kinematic time series calculated by Gipsy and PRIDE PPP-AR software revealing consistent horizontal positioning accuracy (±0.05 m in the East/North components) and coherent kinematic trends as shown in Fig. 10. Specifically, the motion changes at the day boundary in the Gipsy results align with the single-day solution time series from PRIDE PPP-AR, both exhibiting significant step-like variations (amplitude ~0.03 m). Notably, the continuous processing strategy yields smooth transitions across day boundaries, effectively eliminating boundary artifacts caused by parameter resets in single-day solutions. These findings highlight that adopting multi-day continuous processing strategies significantly enhances data continuity, thereby providing more robust observational constraints for monitoring pre-seismic deformation precursors.

4. Conclusions

Capturing reliable precursors to achieve short-term earthquake prediction is a long-standing pursuit in seismology. The approach proposed by Bletery and Nocquet (2023) provides a valuable strategy, yet ensuring the accuracy of time series is a crucial prerequisite for investigating precursory signals. Directly concatenating high-rate time series obtained from the NGL website or applications on the single-day processing strategy may result in discontinuities at the day boundary, potentially affecting the results. Therefore, we recommend first obtaining a high-rate GNSS time series continuously processed for the 48 h preceding the earthquake before applying their method. This should be followed by removing the CME and other potential factors to obtain data without interference, which can then be used for stacking calculations to investigate the precursors of large earthquakes. Following the above strategies, we find that there is no significant preseismic slip that would lead to deformation exceeding the GNSS data noise level before the Kahramanmaraş event. In the future, combining long-term (a few months before large earthquakes) GNSS observation data with seismological observations to investigate precursory anomalies and the earthquake nucleation process may be a good choice (Kwiatek et al., 2023; Peng and Lei, 2025; Picozzi et al., 2023).

CRediT authorship contribution statement

Jingqi Wang: Writing – original draft, Methodology, Investigation, Formal analysis. **Rumeng Guo:** Writing – review & editing, Writing – original draft, Project administration, Investigation, Funding acquisition, Formal analysis, Conceptualization. **Jianqiao Xu:** Writing – review & editing, Funding acquisition. **Heping Sun:** Writing – review & editing, Funding acquisition.

Availability statement

The raw GNSS data are provided by Türkiye Ulusal Sabit GNSS Ağı-Aktif (TUSAGA-Active) System (https://www.tusaga-aktif.gov.tr/Web/DepremVerileri.aspx) and are processed with the PRIDE PPP-AR software. The PRIDE PPP-AR is available at https://github.com/PrideLab/PRIDE-PPPAR. The Bletery and Nocquet's code and results are available at https://zenodo.org/records/8064086. The scripts and data utilized in this study are available on Zenodo (https://doi.org/10.5281/zenodo.14173350). The hypocenter location is provided from the relocated AFAD catalog by Anthony Lomax (https://doi.org/10.5281/zenodo.7727678).

Declaration of competing interest

The authors declare that they have no known competing financial interests or personal relationships that could have influenced the work reported in this paper.

Author agreement and acknowledgement

We thank Editor Zhigang Peng and two anonymous reviewers for their constructive comments. We thank Prof. Jianghui Geng and Dr. Qiang Wen for their guidances in the use of the PRIDE PPP-AR software. This study was supported by National Science Foundation of China (42025401), Natural Science Foundation of Wuhan (2024040701010065), Knowledge Innovation Program of Wuhan-Shuguang Project (2023010201020281), Open Fund of Hubei Luojia Laboratory (230100015 and 220100033), Innovation Group Project of Natural Science Foundation of Hubei Province (2023AFA040), and National Precise Gravity Measurement Facility, Huazhong University of Science and Technology, Wuhan 430074, China.

References

Barbot, S., Luo, H., Wang, T., Hamiel, Y., Piatibratova, O., Javed, M.T., Braitenberg, C., Gurbuz, G., 2023. Slip distribution of the february 6, 2023 M_W 7.8 and M_W 7.6, Kahramanmaraş, Turkey earthquake sequence in the East Anatolian Fault Zone. Seismica 2 (3). https://doi.org/10.26443/seismica.v2i3.502.

Bedford, J.R., Moreno, M., Deng, Z., Oncken, O., Schurr, B., John, T., Báez, J.C., Bevis, M., 2020. Months-long thousand-kilometre-scale wobbling before great subduction earthquakes. Nature 580 (7805), 628–635. https://doi.org/10.1038/s41586-020-2212-1.

Bian, Y., Yue, J., Ferreira, V.G., Cong, K., Cai, D., 2021. Common mode component and its potential effect on GPS-inferred crustal deformations in Greenland. Pure Appl. Geophys. 178 (5), 1805–1823.
Bletery, Q., Nocquet, J.-M., 2023. The precursory phase of large earthquakes. Science 381 (6655), 297–301. https://doi.org/10.1126/science.adg2565.
Bletery, Q., Nocquet, J.-M., 2025. Do large earthquakes start with a precursory phase of slow slip? Seismica 3 (2). https://doi.org/10.26443/seismica.v3i2.1383.
Bolton, D.C., Marone, C., Saffer, D., Trugman, D.T., 2023. Foreshock properties illuminate nucleation processes of slow and fast laboratory earthquakes. Nat. Commun. 14 (1), 3859. https://doi.org/10.1038/s41467-023-39399-0.
Bradley, K., Hubbard, J., 2023. Earthquake precursors? Not so fast. Earthquake Insights. https://doi.org/10.62481/310cc439.
Bouchon, M., Durand, V., Marsan, D., Karabulut, H., Schmittbuhl, J., 2013. The long precursory phase of most large interplate earthquakes. Nat. Geosci. 6 (4), 299–302. https://doi.org/10.1038/ngeo1770.
Bouchon, M., Karabulut, H., Aktar, M., Özalaybey, S., Schmittbuhl, J., Bouin, M.-P., 2011. Extended nucleation of the 1999 M_w 7.6 Izmit earthquake. Science 331 (6019), 877–880. https://doi.org/10.1126/science.1197341.
Bowman, D.D., King, G.C.P., 2001. Accelerating seismicity and stress accumulation before large earthquakes. Geophys. Res. Lett. 28 (21), 4039–4042. https://doi.org/10.1029/2001GL013022.
Bürgmann, R., 2023. Reliable earthquake precursors? Science 381 (6655), 266–267. https://doi.org/10.1126/science.adi8032.
Caballero, E., Chounet, A., Duputel, Z., Jara, J., Twardzik, C., Jolivet, R., 2021. Seismic and aseismic fault slip during the initiation phase of the 2017 M_W= 6.9 Valparaíso earthquake. Geophys. Res. Lett. 48 (6), e2020GL091916. https://doi.org/10.1029/2020GL091916.
Dodge, D.A., Beroza, G.C., Ellsworth, W.L., 1996. Detailed observations of California foreshock sequences: Implications for the earthquake initiation process. J. Geophys. Res. Solid Earth 101 (B10), 22371–22392. https://doi.org/10.1029/96JB02269.
Ellsworth, W.L., Bulut, F., 2018. Nucleation of the 1999 Izmit earthquake by a triggered cascade of foreshocks. Nat. Geosci. 11 (7), 531–535. https://doi.org/10.1038/s41561-018-0145-1.
Emre, Ö., Duman, T.Y., Özalp, S., Şaroğlu, F., Olgun, Ş., Elmacı, H., Çan, T., 2018. Active fault database of Turkey. Bull. Earthquake Eng. 16 (8), 3229–3275. https://doi.org/10.1007/s10518-016-0041-2.
Geng, J., Chen, X., Pan, Y., Mao, S., Li, C., Zhou, J., Zhang, K., 2019. Pride PPP-AR: an open-source software for GPS PPP ambiguity resolution. GPS Solut. 23, 1–10. https://doi.org/10.1007/s10291-019-0888-1.
Geng, J., Wen, Q., Chen, G., Dumitraschkewitz, P., Zhang, Q., 2024. All-frequency IGS phase clock/bias product combination to improve PPP ambiguity resolution. J. Geod. 98 (6), 48. https://doi.org/10.1007/s00190-024-01865-y.
Geng, J., Zhang, Q., Li, G., Liu, J., Liu, D., 2022. Observable-specific phase biases of Wuhan multi-GNSS experiment analysis center's rapid satellite products. Satell. Navig. 3 (1), 23. https://doi.org/10.1186/s43020-022-00084-0.
Hirose, H., Kato, A., Kimura, T., 2024. Did short-term preseismic crustal deformation precede the 2011 great Tohoku-oki earthquake? An examination of stacked Tilt records. Geophys. Res. Lett. 51 (12), e2024GL109384. https://doi.org/10.1029/2024GL109384.
Jia, Z., Jin, Z., Marchandon, M., Ulrich, T., Gabriel, A.-A., Fan, W., Shearer, P., Zou, X., Rekoske, J., Bulut, F., 2023. The complex dynamics of the 2023 Kahramanmaraş, Turkey, M_W 7.8-7.7 earthquake doublet. Science 381 (6661), 985–990. https://doi.org/10.1126/science.adi0685.
Kaneko, Y., Nielsen, S.B., Carpenter, B.M., 2016. The onset of laboratory earthquakes explained by nucleating rupture on a rate-and-state fault. J. Geophys. Res. Solid Earth 121 (8), 6071–6091. https://doi.org/10.1002/2016JB013143.
Kwiatek, G., Martínez-Garzón, P., Becker, D., Dresen, G., Cotton, F., Beroza, G.C., Acarel, D., Ergintav, S., Bohnhoff, M., 2023. Months-long seismicity transients preceding the 2023 M_W 7.8 Kahramanmaraş earthquake, Türkiye. Nat. Commun. 14, 7534. https://doi.org/10.1038/s41467-023-42419-8.
Lara, P., Bletery, Q., Ampuero, J.P., Inza, A., Tavera, H., 2023. Earthquake early warning starting from 3 s of records on a single station with machine learning. J. Geophys. Res. Solid Earth 128 (11), e2023JB026575. https://doi.org/10.1029/2023JB026575.
Li, W., Li, F., Zhang, S., Lei, J., Zhang, Q., Yuan, L., 2019. Spatiotemporal filtering and noise analysis for regional GNSS network in Antarctica using independent component analysis. Remote Sens. 11 (4), 386.
Lomax, A., 2023. Precise, NLL-SSST-Coherence Hypocenter Catalog for the 2023 M_W 7.8 and M_W 7.6 SE Turkey Earthquake Sequence Data Sets. Zenodo. https://doi.org/10.5281/zenodo.7699882.
Mai, P.M., Aspiotis, T., Aquib, T.A., Cano, E.V., Castro-Cruz, D., Espindola-Carmona, A., Li, B., Li, X., Liu, J., Matrau, R., 2023. The destructive earthquake doublet of 6 February 2023 in South-central Türkiye and Northwestern Syria: Initial observations and analyses. The Seismic Record 3 (2), 105–115. https://doi.org/10.1785/0320230007.
Melgar, D., et al., 2023. Sub- and super-shear ruptures during the 2023 M_W 7.8 and M_W 7.6 earthquake doublet in SE Türkiye. Seismica 2 (3). https://doi.org/10.26443/seismica.v2i3.387.
Montagner, J.-P., Juhel, K., Barsuglia, M., Ampuero, J.P., Chassande-Mottin, E., Harms, J., Whiting, B., Bernard, P., Clévédé, E., Lognonné, P., 2016. Prompt gravity signal induced by the 2011 Tohoku-Oki earthquake. Nat. Commun. 7 (1), 13349. https://doi.org/10.1038/ncomms13349.
Peng, Z., Lei, X., 2025. Physical mechanisms of earthquake nucleation and foreshock: cascade triggering, aseismic slip, or fluid flows? Earthq. Res. Adv. 5 (2), 100349. https://doi.org/10.1016/j.eqrea.2024.100349.
Picozzi, M., Iaccarino, A.G., Spallarossa, D., 2023. The preparatory process of the 2023 M_W 7.8 Türkiye earthquake. Sci. Rep. 13, 17853. https://doi.org/10.1038/s41598-023-45073-8.
Pritchard, M.E., Allen, R.M., Becker, T.W., Behn, M.D., Brodsky, E.E., Bürgmann, R., Ebinger, C., Freymueller, J.T., Gerstenberger, M., Haines, B., Kaneko, Y., 2020. New opportunities to study earthquake precursors. Seismolo. Soc. Am. 91 (5), 2444–2447. https://doi.org/10.1785/0220200089.
Rietsch, E., 1980. Estimation of the signal-to-noise ratio of seismic data with an application to stacking. Geophys. Prospect. 28 (4), 531–550. https://doi.org/10.1111/j.1365-2478.1980.tb01241.x.
Roeloffs, E.A., 2006. Evidence for aseismic deformation rate changes prior to earthquakes. Annu. Rev. Earth Planet Sci. 34 (1), 591–627. https://doi.org/10.1146/annurev.earth.34.031405.124947.
Ruiz, S., Metois, M., Fuenzalida, A., Ruiz, J., Leyton, F., Grandin, R., Vigny, C., Madariaga, R., Campos, J., 2014. Intense foreshocks and a slow slip event preceded the 2014 Iquique M_W 8.1 earthquake. Science 345 (6201), 1165–1169. https://doi.org/10.1126/science.1256074.
Shreedharan, S., Bolton, D.C., Rivière, J., Marone, C., 2020. Preseismic fault creep and elastic wave amplitude precursors scale with lab earthquake magnitude for the continuum of tectonic failure modes. Geophys. Res. Lett. 47 (8), e2020GL086986. https://doi.org/10.1029/2020GL086986.
Tan, O., 2021. A homogeneous earthquake catalogue for Turkey. Nat. Hazards Earth Syst. Sci. 21 (7), 2059–2073. https://doi.org/10.5194/nhess-21-2059-2021.
Wang, K., Peng, Z., Liang, S., Luo, J., Zhang, K., He, C., 2024. Migrating foreshocks driven by a slow slip event before the 2021 M_W 6.1 Yangbi, China earthquake. J. Geophys. Res. 129, e2023JB027209. https://doi.org/10.1029/2023JB027209.
Xu, L., Mohanna, S., Meng, L., Ji, C., Ampuero, J.-P., Yunjun, Z., Hasnain, M., Chu, R., Liang, C., 2023. The overall-subshear and multi-segment rupture of the 2023 M_W7. 8 Kahramanmaraş, Turkey earthquake in millennia supercycle. Commun. Earth Environ. 4 (1), 379. https://doi.org/10.1038/s43247-023-01030-x.
Zhang, Y., Tang, X., Liu, D., Taymaz, T., Eken, T., Guo, R., Zheng, Y., Wang, J., Sun, H., 2023. Geometric controls on cascading rupture of the 2023 Kahramanmaraş earthquake doublet. Nat. Geosci. 16 (11), 1054–1060. https://doi.org/10.1038/s41561-023-01283-3.